

# Optical trapping of nanoparticles by full solid-angle focusing

Vsevolod Salakhutdinov,<sup>1,2</sup> Markus Sondermann,<sup>1,2,\*</sup> Luigi Carbone,<sup>3</sup>  
 Elisabeth Giacobino,<sup>4,1</sup> Alberto Bramati,<sup>4</sup> and Gerd Leuchs<sup>1,2,5</sup>

<sup>1</sup>*Max Planck Institute for the Science of Light,  
 Guenther-Scharowsky-Str. 1/ building 24, 91058 Erlangen, Germany*

<sup>2</sup>*Friedrich-Alexander-Universität Erlangen-Nürnberg (FAU),  
 Department of Physics, Staudtstr. 7/B2, 91058 Erlangen, Germany*

<sup>3</sup>*CNR NANOTEC-Istituto di Nanotecnologia U.O. Lecce,  
 c/o Polo di Nanotecnologia-Campus Ecotekne, via Monteroni, 73100 Lecce, Italy*

<sup>4</sup>*Laboratoire Kastler Brossel, UPMC-Sorbonne Universités,  
 CNRS, ENS-PSL, Research University, Collège de France,  
 4 place Jussieu, case 74 F-75005 Paris, France*

<sup>5</sup>*Department of Physics, University of Ottawa, Ottawa, Ont. K1N 6N5, Canada  
 (Dated: February 19, 2022)*

Optical dipole-traps are used in various scientific fields, including classical optics, quantum optics and biophysics. Here, we propose and implement a dipole-trap for nanoparticles that is based on focusing from the full solid angle with a deep parabolic mirror. The key aspect is the generation of a linear-dipole mode which is predicted to provide a tight trapping potential. We demonstrate the trapping of rod-shaped nanoparticles and validate the trapping frequencies to be on the order of the expected ones. The described realization of an optical trap is applicable for various other kinds of solid-state targets. The obtained results demonstrate the feasibility of optical dipole-traps which simultaneously provide high trap stiffness and allow for efficient interaction of light and matter in free space.

## I. INTRODUCTION

About fifty years ago optical forces have been used for the first time in trapping and localizing particles [1]. Since then, optical traps have become a workhorse in many fields of science, not least in atomic physics, quantum optics and optomechanics. In these areas, experiments are typically conducted in the Rayleigh regime, where the size of the trapped particle is much smaller than the wavelength of the trapping beam. In this case, the particle acts as a point-dipole, and the trapping potential scales with the product of the particle's polarizability and the squared modulus of the spatially varying amplitude of the electric field.

Choosing a specific particle, the depth of the trapping potential is maximized by maximizing the field amplitude of the focused trapping beam. The optical modes yielding the maximum possible field amplitude at constant input power are electric-dipole modes [2]. These modes have been suggested previously to maximize the interaction of light and single atoms in free space [3–6]. In this paper, we demonstrate for the first time a dipole trap generated with such a mode.

The key aspect in the generation of an electric-dipole wave is the focusing of a suitably shaped light mode with optics covering the entire solid angle. Such an optical element can be realized with a parabolic mirror (PM) that is much deeper than its focal length [5]. As outlined in the next section, optical tweezers based on a dipole wave not only result in a deeper trapping potential, but also in high trap frequencies.

There are several current research topics which could benefit from an optical trap realized with a deep PM. Recently, there has been experimental progress in

the trapping of nanoparticles in the context of cavity-free opto-mechanics [7–12], where stiffer traps could help in reaching the quantum regime of the particle's motion [13]. Another motivation is the application of the free-space light-matter coupling scheme proposed in Ref. [6] for solid-state quantum targets. By trapping such targets in an optical dipole-trap, the actual excitation of the freely levitated quantum emitter would not suffer from disturbances induced by refractive index boundaries as present when focusing onto emitters located in a solid-state host medium. For example, Ref. [14] discusses the detrimental effects induced by boundaries between different dielectrics when focusing onto buried InAs semiconductor quantum dots. Furthermore, the fluorescence collected by a deep PM from a single photon source can be extremely high, as exemplified for a single ion effectively radiating as an isotropic point source [15]. For a linear-dipole emitter oriented along the PM's axis, the collection efficiency can be close to unity even for a PM of finite depth.

In the next section, we describe the basic features of optical tweezers implemented by focusing via a deep PM, highlighting its favorable figures of merit. Section III reports on the experimental implementation of a PM dipole trap. Finally, we provide an outlook to future work.

## II. CONCEPT OF A DEEP PARABOLIC MIRROR DIPOLE TRAP

In the past few years spherical mirrors and parabolic mirrors (PMs) have been considered in the literature and used for trapping micro- and nano-objects. In Ref. [16] an array of parabolic mirrors with half opening angles of 38° has been used to trap particles in a fluid. Analogously micro-fabricated spherical

---

\* markus.sondermann@fau.de

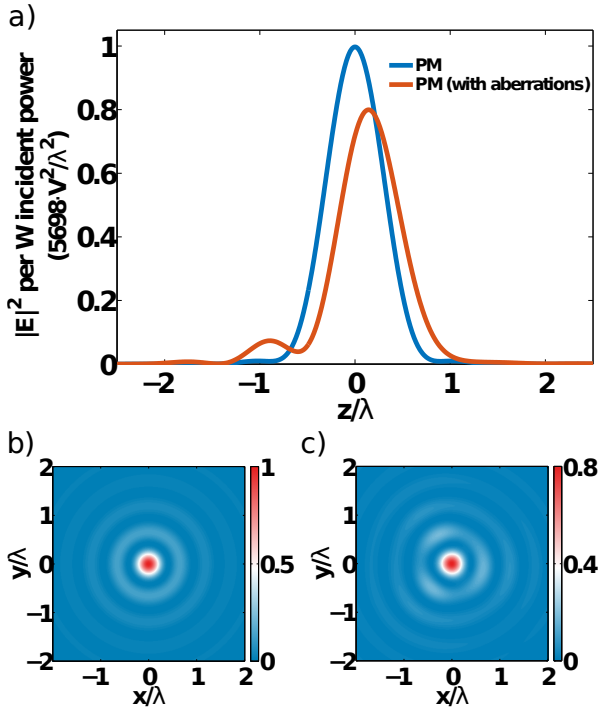


FIG. 1. Simulated intensity distributions for a dipole trap based on a deep PM (see text for all parameters). The PM is illuminated by a radially polarized doughnut mode. (a) Intensity distribution along the optical axis of the PM. The blue curve denotes the case of an aberration free mirror, the orange curve is based on a simulation accounting for the aberrations of the mirror used in the experiments and a wavelength  $\lambda = 1064 \text{ nm}$ . (b,c) Intensity distribution in the plane perpendicular to the optical axis at the axial position with highest intensity for the diffraction limited case (b) and accounting for aberrations (c).

mirrors have been proposed for the implementation of dipole traps for neutral atoms [17], whereas the experimental implementation of a single such trap was demonstrated recently [18]. However, also there the solid angle spanned by the trapping mirror was still fairly small.

In this article we analyze and use a PM design with a depth much larger than the focal length. The mirror geometry is the same as used in Refs. [15, 19]. A focal length of  $f = 2.1 \text{ mm}$  and an aperture radius of  $10 \text{ mm}$  result in a half-opening angle of  $135^\circ$  and a depth of the parabola of  $11.9 \text{ mm}$ . This yields a coverage of 94% of the solid angle relevant for a linear dipole oriented along the axis of the PM. To produce a dipole wave, the PM is illuminated with a radially polarized mode with the amplitude distribution  $A(r) \sim r \cdot \exp(-r^2/w^2)$  (so-called ‘doughnut’ mode). When choosing the beam radius to be  $w = 2.26f$  one obtains a close-to ideal dipole wave after reflection of the doughnut mode at the PM’s surface [20]. The advantages of radially polarized modes for optical trapping – a tighter potential in radial direction and the absence of scattering forces on the optical axis – have been discussed earlier [21], although not in the context of a dipole mode.

We now describe the benefits of an optical dipole trap based upon focusing with a deep PM. The trap-

ping potential is given by the relation  $U(\vec{q}) = -\alpha/2 \cdot |E(\vec{q})|^2$  [22], where  $\alpha$  is the polarizability of the particle and  $E(\vec{q})$  the spatially varying amplitude of the electric field used for trapping at position  $\vec{q} = (x, y, z)$ . As outlined above, by increasing the maximum field amplitude  $E(\vec{q})$ , the depth of the trapping potential increases, thus achieving the maximum potential depth in free space with an electric-dipole wave [2].

As discussed in Ref. [20], the energy fraction of dipole radiation contained in a focused optical beam is limited by the solid angle covered by the focusing optics. More precisely, the relevant quantity is the solid angle  $\Omega = \int D(\vartheta) \sin \vartheta d\varphi d\vartheta$  obtained by weighting the solid angle used for focusing with the desired angular dipole radiation pattern  $D(\vartheta) = \sin^2 \vartheta$  for a linear dipole. By focusing from full solid angle  $\Omega$  is maximized to  $8\pi/3$  [20]. For the PM used here  $\Omega = 0.94 \cdot 8\pi/3$ . According to Ref. [20] one has  $|E(0)|^2 \propto \Omega \eta^2$  with  $0 \leq \eta \leq 1$  parametrizing the similarity of the incident radiation pattern with a dipole wave and the mirror’s focus located at  $\vec{q} = 0$ . For the doughnut mode used here one has  $\eta = 0.98$ . In other words, for a given power the PM design used here can deliver 90% of the maximum possible potential depth (cf. Ref. [23]).

Next we estimate the achievable trapping frequencies. We compute the focal intensity distribution for our chosen mirror geometry and incident beam, assuming an aberration free PM. The simulations were performed using a generalization of the method by Richards and Wolf [24]. The results are reported in Fig. 1(a) and (b). In the vicinity of its minimum, the trapping potential can be approximated by the harmonic potential  $U(\vec{q}) \approx k \cdot q^2/2$ , where  $k = m\omega^2$  is the trap stiffness,  $m$  is the trapped particle’s mass and  $\omega$  is the trap frequency.  $k$  is obtained from fitting axial and radial cuts through the focus to the harmonic potential  $U(z)$  and  $U(r)$ , respectively. We obtain  $k_z = 5/\lambda^2 \cdot \alpha |E(0)|^2$  for the trap stiffness in axial direction and  $k_r = 15/\lambda^2 \cdot \alpha |E(0)|^2$  in radial direction. A possible influence to the trapping potential of the polarization components perpendicular to the optical axis can be neglected due to their low magnitude in relation to the longitudinal field. The transverse field components reach a maximum value of about 3% of the focal intensity approximately at  $0.6 \lambda$  distance to the focus. Along the optical axis the off-axis field components vanish due to symmetry reasons when focusing a radially polarized beam.

To gauge our results, we compare the stiffnesses obtained for the deep PM to the ones obtained when focusing a linearly polarized fundamental Gaussian mode with a lens to a beam waist  $w$  and a Rayleigh length  $z_R$ . For such a mode the trap stiffnesses are derived in Ref. [10] to be  $k_{z,\text{Gauss}} = \alpha |E(0)|^2 / z_R^2$  and  $k_{r,\text{Gauss}} = \alpha |E(0)|^2 / w^2$ . In an attempt to compare to a typical example we choose  $\lambda = 1064 \text{ nm}$  and the beam parameters from Ref. [10] which are  $w \approx 0.54 \mu\text{m}$  and  $z_R \approx 1.36 \mu\text{m}$ , obtained with an  $\text{NA}=0.8$  objective. The resulting trap stiffnesses are lower by a factor of 4 and 8 in radial and axial direction, respectively, as compared to what we obtain for the deep PM. Moreover, this calculation assumes

the same maximum focal intensity  $|E(0)|^2$  for the focused Gaussian beam and for the PM. When comparing the stiffnesses for the same incident power in the two cases, the improvement for the deep PM is even more pronounced, since the fraction of the dipole weighted solid angle covered by an  $\text{NA}=0.8$  objective is only about  $\Omega = 0.25 \cdot 8\pi/3$  and the maximum focal intensity is increased by a factor of 3.6 when using the deep PM. In total, this suggests that with a deep PM the trap stiffness can be improved by up to one order of magnitude in the ideal case. Other measures to improve the stiffness such as using a standing wave trap or a cavity are not considered here as we do not want to change the spectrum of modes of free space, retaining the highest possible frequency bandwidth for coupling to a trapped quantum target.

Experimentally, CdSe/CdS dots-in-rods (DRs) [25] were trapped in air at normal ambient pressure. For estimating the polarizability of these particles we neglect the spherical CdSe core, which makes a negligible contribution to the total volume. The DRs used in the experiment have a cylindrical shape with a length of 58 nm and a diameter of 7 nm. Within good approximation, these particles can be treated as point-like, since in all spatial directions their extent is much smaller than the wavelength of the trapping laser. Furthermore, using the same wavelength even larger particles have been treated successfully as point-like scatterers in recent literature [8, 10, 13]. Since there is no closed analytic expression for the polarizability of a dielectric cylinder, we approximate the CdS rods as prolate spheroids. An expression for the polarizability of prolate spheroids is found in e.g. Ref.[26]. For a refractive index of CdS at 1064 nm of  $n_{\text{CdS}} = 2.344$  we arrive at a polarizability  $\alpha = 5.28 \cdot 10^{-35} \text{ Cm}^2/\text{V}$ . From this value we expect a potential depth of  $|U(0)| \approx k_B \cdot 9600 \text{ K}$  for an incident power of 1 W. Under ambient conditions, the trapped particle thermalizes to room temperature due to collisions with air molecules [10]. Hence, we expect that the minimal power for trapping is about 32 mW.

For completeness we note that also the excitonic optical transition has a finite polarizability. Assuming a center wavelength of  $\lambda_{\text{exc}} = 595 \text{ nm}$  and a radiative life time of  $\tau = 15 \text{ ns}$  as found for the DRs used here, we calculate an excitonic polarizability of  $\alpha_{\text{exc}} = 1.7 \cdot 10^{-39} \text{ Cm}^2/\text{V}$  when focusing at 1064 nm [27]. This polarizability is four orders of magnitude below the one estimated for the rod material and can therefore be neglected.

### III. EXPERIMENTAL REALIZATION

In the experiment we use an aluminum PM made by diamond turning (Fraunhofer IOF, Jena), fabricated with the dimensions given above. The surface of the mirror exhibits deviations from a parabola. These surface deviations are measured by interferometry [28]. In general, such deviations distort the focus, leading to a reduced depth of the optical trapping potential as well as reduced curvatures of the potential. In order to estimate the influence of these deviations, we per-

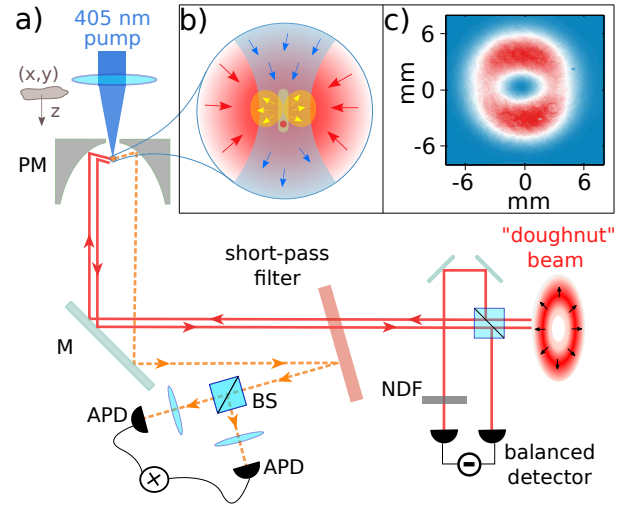


FIG. 2. (a) Scheme of the experimental setup. A radially polarized ‘doughnut’ mode ( $\lambda = 1064 \text{ nm}$ , intensity profile in panel (c)) is focused by a deep PM. Fine tuning of the beam’s angular alignment is achieved by a mirror (M). The trapped nanoparticles are excited by a pulsed 405 nm laser (1 MHz repetition rate, average power  $\sim 4.5 \mu\text{W}$ ), which is focused onto the trapped particles through a bore hole at the PM’s vertex, see panel (b) for illustration. The photons emitted by the dot-in-rod nanoparticles (595 nm center wavelength) are collimated by the PM and split from the infrared light by a reflective short pass filter (776 nm cutoff wavelength). A beam splitter (BS) directs the fluorescence photons onto two avalanche photo diodes (APD) for detecting the presence of trapped particles and measurements of the second order intensity-correlation function. Both APDs are equipped with chromatic filters blocking the 405 nm excitation light. The trapped particles’ motion is analyzed by means of a balanced detector, which delivers the difference signal between the infrared light leaving the parabolic mirror and the incident light. The detection is calibrated by means of a neutral-density filter (NDF) such that the difference signal is canceled out when no particles are trapped.

formed simulations of the focal intensity distribution based on the measured aberrations. The corresponding phase front errors have been incorporated in the simulations by attributing them to the phase front of the incident beam. The results for a wavelength of 1064 nm are given in Fig.1(a) and (c). The maximum intensity in the focal region and consequently the potential depth is reduced by 20%. Accordingly, the minimum power required to trap a single nanorod at room temperature increases to 39 mW. The intensity maximum is shifted along the optical axis of the PM by a negligible amount. The curvatures of the trapping potential are slightly reduced to values of  $k_r = 13.7/\lambda^2 \cdot \alpha E_{\text{max}}^2$  and  $k_z = 3.3/\lambda^2 \cdot \alpha E_{\text{max}}^2$ , with  $E_{\text{max}}$  the field amplitude at the intensity maximum in the presence of aberrations. The rotational symmetry of the intensity distribution in the plane perpendicular to the PM’s optical axis, and hence the symmetry of  $U(r)$ , is hardly disturbed.

The experimental setup is outlined in Fig.2a. A single-mode continuous wave laser operating at 1064 nm (Cobolt Rumba, 2 W output power) is sent through a liquid-crystal based polarization converter

(ArcOptix) and a spatial filter in order to produce a radially polarized doughnut mode. The spatial filter comprises a telescope with a pinhole positioned in the focal plane. The pinhole rejects unwanted higher-order modes and cleans the phase front of the transmitted mode to a large extent. The intensity distribution of the resulting doughnut mode is shown in Fig. 2(c). The rotational symmetry of the mode is slightly perturbed. In order to assess the influence of this perturbation, we characterized the generated doughnut mode by a spatially resolved measurement of the Stokes parameters. Using the same methods and analysis as described in Ref. [23] an overlap  $\eta = 0.95$  with an ideal dipole-mode is obtained. This value is in good agreement with the value assumed in our calculations above and demonstrates a high quality of the radially polarized mode. The doughnut mode incident onto the PM has a beam radius  $w \sim 4.7$  mm.

The DR nanoparticles are delivered to the trapping region with an approach adapted from Refs. [8, 11, 29]. The DR particles are dispersed in toluene and diluted to a concentration of about  $10^{-9}$  mol/l. In a next step this solution is dissolved in methanol with a ratio of 1:100. The resulting solution is sonicated for ten minutes and then transferred into an ultrasonic nebulizer (Omron), from where it is sprayed to the vicinity of the rear side of the PM. Droplets containing DRs diffuse in the air towards the trapping region through an opening at the vertex of the parabola. DRs are then trapped in the focus of the PM.

To detect the motion of the particles in the trap we adapt an approach from Ref. [30] based on the interference of the light of the trapping laser and the light scattered from the trapped object. The PM reflects a huge portion of the incident light back into the direction of incidence. Simultaneously the PM collimates almost the entire light scattered by the trapped particle. Due to the motion of the particle in the trap, the resulting interference signal is varying in time. Since a deep PM acts as an efficient retro-reflector, the back reflected light is much stronger than the scattered counterpart, resulting in a small modulation due to interference on top of a large constant background. Hence, we apply balanced detection by subtracting a reference signal picked off from the trapping laser before it enters the PM, cf. Fig. 2. This allows to measure the trap frequencies as shown below (see also Fig. 4a).

The DR particles are optically excited by a pulsed laser operating at 405 nm wavelength (Alphas, Picopower). The pulse duration of 80 ps is short in comparison to the excitonic life time of about 15 ns, see also Ref. [25]. After initial trapping with a power of 280 mW, the power of the trapping laser is generally decreased in order to reduce photo bleaching of the DRs. It was found that the DR particles are also excited by the trapping laser via two photon absorption. The final trap beam power of 8.5 mW was chosen such that fluorescence induced by two-photon absorption alone is indistinguishable from the noise floor. Under these conditions DRs remained in the trap for a few tens of minutes. Note that the value of

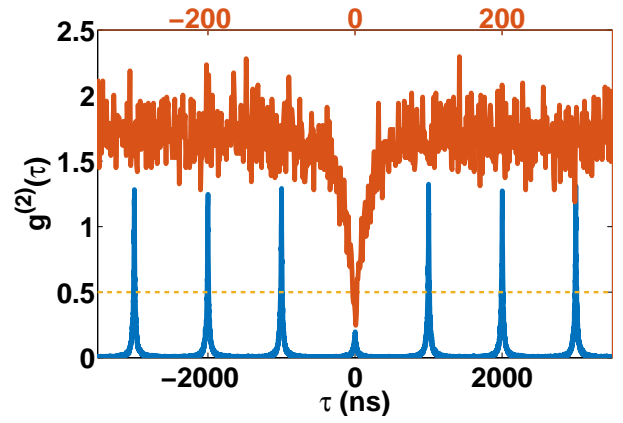


FIG. 3. Second order correlation functions for a single CdSe/CdS nanoparticle. The orange curve corresponds to the function measured when exciting the nanoparticle only with the infrared CW trapping beam at a power level of 370 mW. The blue curve is the correlation function obtained when exciting the nanoparticles with the pulsed 405 nm laser and a trapping beam power of 8.5 mW. The dashed line marks  $g^{(2)}(\tau) = 0.5$ .

8.5 mW is smaller than the 39 mW value at which we expect to loose the DRs from the trap according to the estimation above. This aspect is discussed at the end of this section.

At room temperature the fluorescence spectrum of the DR particles is centered at 595 nm. Fluorescence photons are collimated by the PM (72.4% reflectivity) and separated from the retro-reflected trapping beam and from the pulsed laser by a dichroic mirror. They are detected by two avalanche photo-diodes (Laser-Components, Count 100) working in the Geiger mode. Bandpass filters in front of these diodes (not shown in Fig. 2) block residual light stemming from the trapping and excitation lasers. Overall the net transmission via the PM to the avalanche diodes is 26%, including the losses at the PM's surface and at all other optical components as well as the avalanche diodes' quantum efficiency. Photon detection events are recorded by a time-to-digital converter (quTau from quTools, Munich). From these data we compute the second-order intensity correlation function  $g^{(2)}(\tau)$ , by which we verify whether a single DR particle is emitting.

Figure 3 shows an example of a  $g^{(2)}$  function recorded from the fluorescence of a single DR. For excitation with the trapping beam laser only, as well as with the pulsed laser, the normalized  $g^{(2)}$  function exhibits clear anti-bunching. When pulsed excitation is applied, the trap laser is attenuated to power levels such that no fluorescence due to two-photon absorption is observed. Noteworthy, in both kinds of measurements one obtains  $g^{(2)}(0) \approx 0.2$ . This imperfect antibunching for a single DR is attributed to a small but finite probability for the recombination of more than one exciton [31]. For delays outside the central anti-bunching dip, the  $g^{(2)}$  functions are larger than one. For the DRs this effect is attributed to blinking stemming from the presence of a charged state [32]. At large delays, the measured  $g^{(2)}(\tau)$  approaches unity (not shown in Fig. 3).

In the experiment  $g^{(2)}$  functions with values of



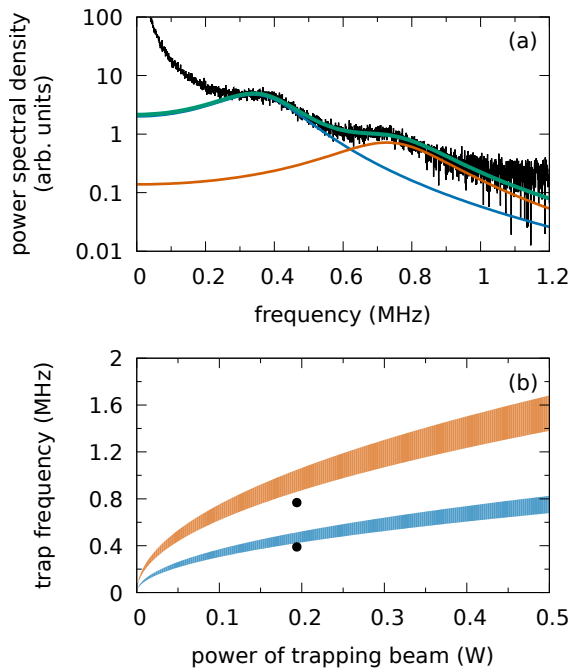


FIG. 4. (a) Power spectral density of the dynamics of the motion of a trapped cluster of DR particles ( $g^{(2)}(0) = 0.9$ ) obtained for a trapping beam power of 194 mW. Black line: experimental data after subtracting the spectral density measured with an empty trap. Green line: Double-Lorentzian fit. Frequencies below 0.3 MHz have been excluded from the fitting procedure. Blue and orange line: Lorentzians attributed to the motion along the PM's optical axis and perpendicular to it, yielding  $\omega_z/2\pi = 0.389$  MHz and  $\omega_r/2\pi = 0.767$  MHz, respectively. (b) Trap frequencies as a function of the trapping beam's power. Shaded areas: Theoretical expectations for  $\omega_r/2\pi$  (orange) and  $\omega_z/2\pi$  (blue). The upper boundary of each area is obtained using the polarizability of a prolate spheroid. The lower border is obtained using the polarizability of a sphere. Both curves account for the aberrations of the PM used in the experiments as well as the experimentally obtained overlap of the doughnut mode with an ideal dipole mode. Black dots: Trap frequencies obtained from the spectrum in (a).

$g^{(2)}(0) > 0.5$  are obtained very frequently, giving the indication that clusters made of DRs are trapped. This can be explained by the fact that methanol, which was used to dilute the DR solution favors DRs aggregation and cluster formation [33]. In view of this it is most likely that the single photon emitters studied above are also made of small clusters of DRs, with only one DR emitting single photons, the other ones being damaged and not emitting anymore.

This clustering effect can also explain the difference between the calculated minimal trapping power and the significantly lower power at which particles could be trapped stably, because a cluster has a larger overall polarizability than a single DR. If one assumes that clusters are made of at least 5 to 7 DRs the low observed trapping power is in good agreement with the calculated one [34].

Finally, we discuss the trap frequencies achieved in the experiments with the PM based optical trap. The frequencies are identified by fitting a sum of two

Lorentzians  $S(f) = \sum_{i=r,z} A_i / [(f^2 - f_i^2)^2 + f^2 \gamma_i^2]$  to power spectra of the signal acquired with the balanced detector, cf. Fig. 2. Here,  $f_i = \omega_i/2\pi$  represent the trap frequencies, the  $\gamma_i$  denote damping terms and the  $A_i$  are used as fit constants (see e.g. Ref. [7]). Figure 4(a) shows the outcome of such a procedure for the case of trapping a cluster. The resulting trap frequencies are compared to the ones expected from calculations in Fig. 4(b). The experimental values are about 10% lower than the ones calculated when assuming a spherical shape. A sphere is likely to be a good approximation for the geometry of a cluster of particles. Nevertheless, one cannot ensure perfect spherical symmetry nor guarantee a homogeneous distribution of mass within a cluster. Therefore, witnessing some deviations in the experiment is not surprising. Another potential origin of discrepancies on the few-percent level could be found in the residual aberrations of the optical elements in the beam path. The deviation of 25% to the trap frequency for a prolate spheroid is more pronounced. On the other hand, the ratio  $f_r/f_z \approx 2$  is the one expected from  $\sqrt{k_r/k_z}$  when taking into account the curvatures of the focal intensity distribution in the presence of the aberrations of the PM. We therefore conclude that our optical trap has a high stiffness, with performances in good agreement with our model.

#### IV. OUTLOOK

We have demonstrated the trapping of nanoparticles in a deep PM via an optical dipole trap, together with the collection of the light emitted by the trapped particles. This result shows the feasibility of an efficient interaction between solid state targets and the light field in free space, and opens the way to the study of solid-state quantum objects without any disturbance induced by a host medium. As a next step, one can envision a setup incorporating two dipole waves: one for trapping the particle, the second one for driving the optical transition of interest.

As test particles we have used CdSe/CdS dot-in-rods. These objects are known to emit with a radiation pattern strongly resembling a linear dipole [25]. Therefore, we expect high efficiencies in collecting the fluorescence photons emitted by these DRs with a deep PM. Besides that, the linear-dipole property of the excitonic transitions of the used DRs makes them suitable candidates for efficient interaction with a dipole wave. For these purposes the dipole axis, which is parallel to the rod axis, has to be aligned along the PM's optical axis, as envisaged in Fig. 2(b). This should occur in a natural way due to the dominating longitudinal electric field vector created by the focused radially polarized trapping beam, which polarizes the rod material. Recent calculations for elongated nanoparticles support this expectation [35].

Moreover a characterization of the trapping dynamics at a significantly reduced pressure should solidify the observed increase of the magnitude of the trap frequencies in comparison to microscope-objective based optical traps further. Already at the current stage,

the measured trap frequencies hint at a trap stiffness unprecedented in free-space focusing.

Under vacuum conditions, the removal of heat from a trapped particle is inefficient, since the collisions with air molecules are less frequent. Besides the well-known consequences for the particle motion, the particle might melt due to heating by the absorption of the trapping light. The latter effect could be especially severe in the tight focusing condition found in a deep PM. Recently, the melting of levitated particles by absorption of the trap-laser light was observed in a low-pressure environment [11]. Therein, this effect has been proven to be especially significant for micrometer-sized spheres and much less for nanospheres of 100 nm diameter. We therefore do not expect this effect for a single DR particle, whose volume is about five to two orders of magnitude smaller, respectively. Indeed, in combination with dedicated

cooling techniques [7, 36], reaching low temperatures for the trapped particle's motion [13] appears to be feasible with a dipole trap based on a deep parabolic mirror.

## FUNDING INFORMATION

G.L. acknowledges financial support from the European Research Council via the Advanced Grant 'PACART'.

## ACKNOWLEDGMENTS

The authors acknowledge fruitful discussions with M. Chekhova, M. Manceau and M. Sytnyk.

- 
- [1] A. Ashkin, *Phys. Rev. Lett.* **24**, 156 (1970).
  - [2] I. M. Basset, *Journal of Modern Optics* **33**, 279 (1986).
  - [3] S. Quabis, R. Dorn, M. Eberler, O. Glöckl, and G. Leuchs, *Opt. Comm.* **179**, 1 (2000).
  - [4] S. J. van Enk, *Phys. Rev. A* **69**, 043813 (2004).
  - [5] N. Lindlein, R. Maiwald, H. Konermann, M. Sondermann, U. Peschel, and G. Leuchs, *Laser Physics* **17**, 927 (2007).
  - [6] M. Sondermann, R. Maiwald, H. Konermann, N. Lindlein, U. Peschel, and G. Leuchs, *Appl. Phys. B* **89**, 489 (2007), arxiv:0708.0772.
  - [7] T. Li, S. Kheifets, and M. G. Raizen, *Nature Physics* **7**, 527 (2011).
  - [8] L. P. Neukirch, J. Gieseler, R. Quidant, L. Novotny, and A. N. Vamivakas, *Opt. Lett.* **38**, 2976 (2013).
  - [9] Y. Arita, M. Mazilu, and K. Dholakia, *Nature communications* **4**, 2374 (2013).
  - [10] J. Gieseler, L. Novotny, and R. Quidant, *Nature Physics* **9**, 806 (2013).
  - [11] J. Millen, T. Deesuwana, P. Barker, and J. Anders, *Nature nanotechnology* **9**, 425 (2014).
  - [12] L. P. Neukirch, E. von Haertman, J. M. Rosenholm, and A. N. Vamivakas, *Nature Photonics* **9**, 653 (2015).
  - [13] B. Rodenburg, L. P. Neukirch, A. N. Vamivakas, and M. Bhattacharya, *Optica* **3**, 318 (2016), arXiv:1503.05233.
  - [14] A. N. Vamivakas, A. Yurt, T. Müller, F. H. Köklü, M. S. Ünlü, and M. Atatüre, *New Journal of Physics* **13**, 053056 (2011).
  - [15] R. Maiwald, A. Golla, M. Fischer, M. Bader, S. Heugel, B. Chalopin, M. Sondermann, and G. Leuchs, *Phys. Rev. A* **86**, 043431 (2012).
  - [16] F. Merenda, J. Rohner, J.-M. Fournier, and R.-P. Salathé, *Opt. Express* **15**, 6075 (2007).
  - [17] J. Goldwin and E. A. Hinds, *Opt. Express* **16**, 17808 (2008).
  - [18] A. Roy, A. B. S. Jing, and M. D. Barrett, *New Journal of Physics* **14**, 093007 (2012).
  - [19] M. Fischer, M. Bader, R. Maiwald, A. Golla, M. Sondermann, and G. Leuchs, *Appl. Phys. B* **117**, 797 (2014), arXiv:1311.1982.
  - [20] M. Sondermann, N. Lindlein, and G. Leuchs, arXiv:0811.2098 [physics.optics] (2008).
  - [21] Q. Zhan, *Opt. Express* **12**, 3377 (2004).
  - [22] L. Novotny and B. Hecht, *Principles of nano-optics* (Cambridge university press, 2012).
  - [23] A. Golla, B. Chalopin, M. Bader, I. Harder, K. Mantel, R. Maiwald, N. Lindlein, M. Sondermann, and G. Leuchs, *Eur. Phys. J. D* **66**, 190 (2012), arXiv:1207.3215.
  - [24] B. Richards and E. Wolf, *Proceedings of the Royal Society of London. Series A, Mathematical and Physical Sciences* **253**, 358 (1959).
  - [25] F. Pisanello, L. Martiradonna, G. Leménager, P. Spinicelli, A. Fiore, L. Manna, J.-P. Hermier, R. Cingolani, E. Giacobino, M. De Vittorio, and A. Bramati, *Applied Physics Letters* **96**, 033101 (2010).
  - [26] J. Mihaljevic, S. Slama, R. Röpke, and A. J. Meixner, *Phys. Rev. A* **90**, 013421 (2014).
  - [27] Modeling the excitonic transition as the one of a two-level atom, we write its polarizability  $\alpha_{\text{exc}} = \mu^2 / (2\hbar\Delta)$  [37], where  $\mu$  is the transition's dipole moment and  $\Delta$  the detuning of the trapping laser  $\nu_{\text{trap}} = 2\pi c_0 / \lambda_{\text{trap}}$  from the excitonic resonance  $\nu_{\text{exc}} = 2\pi c_0 / \lambda_{\text{exc}}$ .  $\mu$  is obtained via the equation  $1/\tau = \mu^2 \nu_{\text{exc}}^3 / (3\pi\epsilon_0 \hbar c^3)$ . The value of  $\tau$  is approximated by the exponential decay constant characteristic to the pulsed  $g^{(2)}$  function in Fig. 3.
  - [28] G. Leuchs, K. Mantel, A. Berger, H. Konermann, M. Sondermann, U. Peschel, N. Lindlein, and J. Schwider, *Applied Optics* **47**, 5570 (2008).
  - [29] Y. Minowa, R. Kawai, and M. Ashida, *Opt. Lett.* **40**, 906 (2015).
  - [30] P. Mestres, J. Berthelot, M. Spasenović, J. Gieseler, L. Novotny, and R. Quidant, *Applied Physics Letters* **107**, 151102 (2015), <http://dx.doi.org/10.1063/1.4933180>.
  - [31] S. Vezzoli, S. Shojaii, S. Cialdi, D. Cipriani, F. Castelli, M. G. Paris, L. Carbone, P. D. Cozzoli, E. Giacobino, and A. Bramati, *Optics Communications* **300**, 215 (2013).
  - [32] M. Manceau, S. Vezzoli, Q. Glorieux, F. Pisanello, E. Giacobino, L. Carbone, M. De Vittorio, and A. Bramati, *Phys. Rev. B* **90**, 035311 (2014).
  - [33] Methanol was added to the DR solution which was originally toluene, because it is better adapted for spraying with the ultrasonic nebulizer. However, DRs are surrounded by alkyl chains that render them

soluble in organic solvents, but polar solvents like methanol tend to promote nanoparticle aggregation.

- [34] From observing trapping powers as low as 8.5 mW it can be inferred that the trapped object has a polarizability that is roughly 5 times larger than calculated for a single CdS rod. Therefore, in first approximation one can deduce that the trapped object is a cluster consisting of  $\geq 5$  rods. However, it is questionable whether a cluster can still be described by a prolate spheroid. Modelling such a cluster as a CdS sphere, the volume of this sphere would amount to the volume of 7 rods with the size parameters given in Sec. II.
- [35] M. Li, S. Yan, B. Yao, M. Lei, Y. Yang, J. Min, and D. Dan, *J. Opt. Soc. Am. B* **32**, 468 (2015).
- [36] J. Gieseler, B. Deutsch, R. Quidant, and L. Novotny, *Phys. Rev. Lett.* **109**, 103603 (2012).
- [37] R. Grimm, M. Weidemüller, and Y. B. Ovchinnikov, *Advances In Atomic, Molecular, and Optical Physics* **42**, 95 (2000), arXiv:physics/9902072.